Journal of Applied Polymer Science

Glass fiber coated with graphene constructed through electrostatic self-assembly and its application in poly(lactic acid) composite

Xiande Yin, Jianjun Bao
The State Key Laboratory of Polymer Materials Engineering, Polymer Research Institute of Sichuan University, Chengdu 610065, China
Correspondence to: J. Bao (E-mail: jjbao2000@sina.com)

ABSTRACT: A method to construct glass fiber/graphene material via the electrostatic self-assembly was proposed. The graphene oxide (GO) nanosheets were firstly prepared from graphite according to Hummer's methods. Oppositely charged GO is successfully introduced to the surface of the GF cationized by 3-aminopropyltriethoxysilane (APTES) treatment in the solution with mild agitation. Sequently, glass fibers coated with graphene (GF/CRG) were obtained after chemical reduction. The graphene content was characterized by TGA and XPS tests and the value of about 0.7 wt % was obtained. Composites of poly(lactic acid) and GF/CRG were prepared through melt blending. Thermogravimetric analysis (TGA) results shows that more than 50% graphene remains on the surface of GF after processing, which indicates a strong binding between GF and graphene. GF/CRG has significant influences on crystallization and mechanical property of PLA: the crystallinity of PLA increases from 27.61 to 51.29%; the tensile strength of the PLA–GF/CRG composite is about 63% larger than the pure PLA at the GF/CRG content of 10 wt %. This new method can apply to making composites with high performance. © 2015 Wiley Periodicals, Inc. J. Appl. Polym. Sci. **2016**, *133*, 43296.

KEYWORDS: electrostatic self-assembly; graphene; interfacial crystallization; poly(l-lactic acid) composite; surfaces and interfaces

Received 29 June 2015; accepted 29 November 2015
DOI: 10.1002/app.43296

INTRODUCTION

As a new carbon material, graphene[1,2] (a monolayer of sp^2-hybridized carbon atoms arranged in a two-dimensional lattice) has excited worldwide interest because of its remarkable thermal, mechanical and electronic properties.[3–6] It has large theoretical specific surface area (2630 m^2 g^{-1}), high intrinsic mobility (~200,000 cm^2 v^{-1} s^{-1}), high Young's modulus (~1.0 TPa) and high thermal conductivity (~5000 Wm^{-1} K^{-1}).[7–9] These excellent physical properties make graphene have great potential in the areas of flexible transparent conductive film, supercapacitor and composite materials with high strength and conductivity. However, graphene is lacking of assembly method due to its insolubility. Self-assembly,[10,11] template-assisted[12] method and direct deposition[13] have been put forward to make graphene fiber, graphene foam, porous membrane and so on.[14–17]

Graphene oxide (GO) is prepared from natural graphite by sufficient oxidation and subsequent strong exfoliation.[18] GO has a great number of oxygen-containing functional group such as epoxy, hydroxyl and carboxyl, making it easier to be functionalized than graphene. Due to the ionization of carboxyl, the surface of GO is usually negatively charged. Thus GO is tend to be co-assembled with the positively charged material through electrostatic interaction. Electrostatic self-assembly[19,20] is a well-established strategy to prepare materials with specific structure. It is based on the electrostatic attraction between consecutively adsorbed and oppositely charged species. Ning *et al.*[21] proposed a new method to introduce GO to the surface of amorphous glass fiber (GF) via electrostatic self-assembling of the oppositely charged GO and amino coupling agent modified GF. After reduction they put the GF-CRG to isotactic polypropylene (iPP) and poly(L-lactide) (PLLA), respectively, and observed the formation of transcrystalline structure at the polymers/GF–RGO interface using a polarized light optical microscope equipped with a hot stage. The results indicated a significantly improved nucleation ability of GF-RGO for polymer crystallization.

Polylactide (PLA) is a commercially available, compostable, bio-based, and thermoplastic material that could become a material of choice, due to its high strength and moderate barrier properties.[22] However, some disadvantages, such as relatively low heat-resistance temperature and long processing cycle, respectively, associated with low crystallinity and slow crystallization rate, have limited its wider application. Improving the crystallinity and crystallization rate and controlling the structure and morphology of crystal are practicable ways to promote the thermal stability and mechanical behaviors.[23]

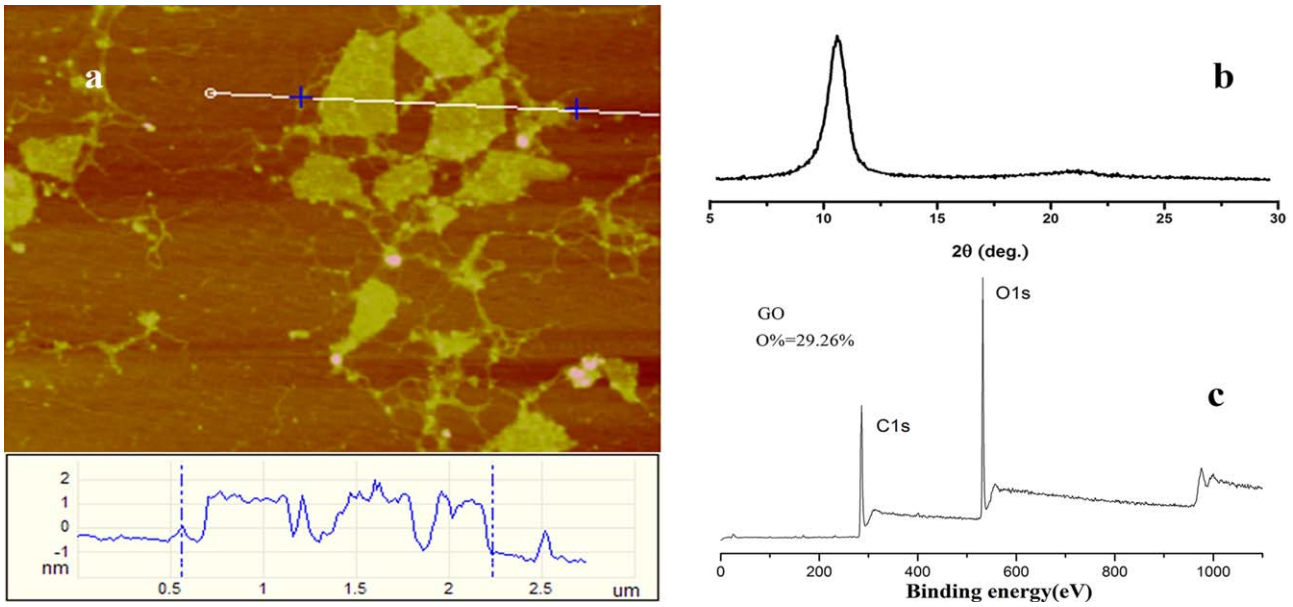

Figure 1. AFM topographic image and height profile of a single layer of GO; XRD pattern of GO. [Color figure can be viewed in the online issue, which is available at wileyonlinelibrary.com.]

In this work, positively charged GF was firstly prepared through the interaction between hydroxyl in GF surface and APTES.[24,25] Subsequently, GO was firmly adsorbed to the modified GF by electrostatic interaction. Our goal is to make a new kind of material and investigate its influences on the PLA composites. Various methods, such as differential scanning calorimeter tests, X-ray diffraction and tensile testing were utilized to study the interfacial crystallization and mechanical behaviors of the composites. It was confirmed that graphene was well kept on the surface of GF. The introduction of GF/CRG greatly increases the crystallinity and mechanical properties of PLA.

EXPERIMENTAL

Materials

Flake graphite with a particle size of 200 meshes was provided by Qingdao Tianheda Graphite, China. Glass fiber (GF) (a fiber diameter of about 11 μm and a length of 4.5 mm) was supplied by Shenzhen Yataida High-Tech. Aminopropyltriethoxysilane (ATPES) with the chemical formula $NH_2(CH_2)_3Si(OC_2H_5)_3$ was provided by Nanjing Xiangqian Chemical. PLA (PLA 4032D, one kind of semicrystalline polymer) purchased from NatureWorks, was used as matrix material with a density of 1.24 g/cm^3. PLA 4032D is characterized by an average molecular weight of 52,000 g mol^{-1} and an *L*/*D* isomer ratio of 90/10. All other reagents were obtained as analytical grade products and used without further purification.

Preparation of GO

Graphene oxide (GO) was prepared from natural graphite by a modification of Hummers and Offeman's method.[26] 0.1 g graphite flakes, 2.3 ml concentrated sulfuric acid and 0.05 g sodium nitrate were added to a reaction vessel immersed in an ice bath to keep the temperature stable at 0–4°C, and then 0.3 g potassium permanganate was added slowly. The oxidation reaction continued at 0–4°C for 2 h and the vessel stood overnight at room temperature. After that the reaction continued at 35°C for 30 min and at 80–90°C for another 15 min successively to fully oxidize graphite into graphite oxide. Graphite oxide was thoroughly washed by hydrogen peroxide, hydrochloric acid and deionized water individually and centrifuged to remove metal ions until pH 7. The graphite oxide was suspended in water and exfoliated through ultrasonication for 1 h. The supernatant was obtained as the GO suspension by centrifugalization.

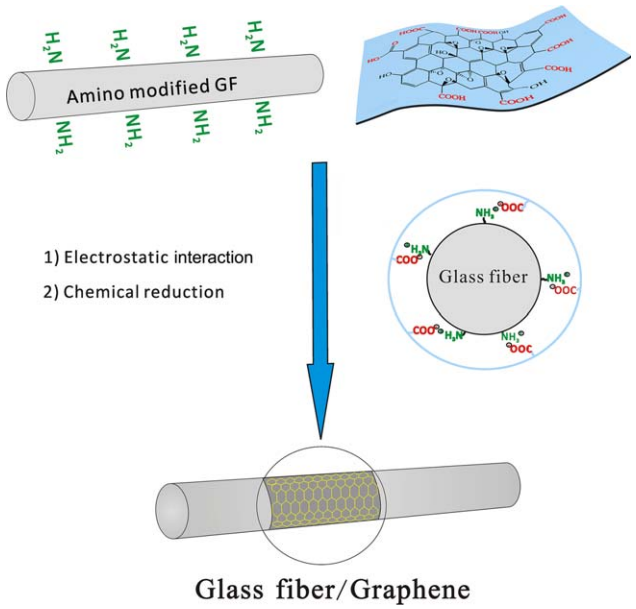

Figure 2. Schematic for electrostatic self-assembly of graphene and cationized glass fiber. [Color figure can be viewed in the online issue, which is available at wileyonlinelibrary.com.]

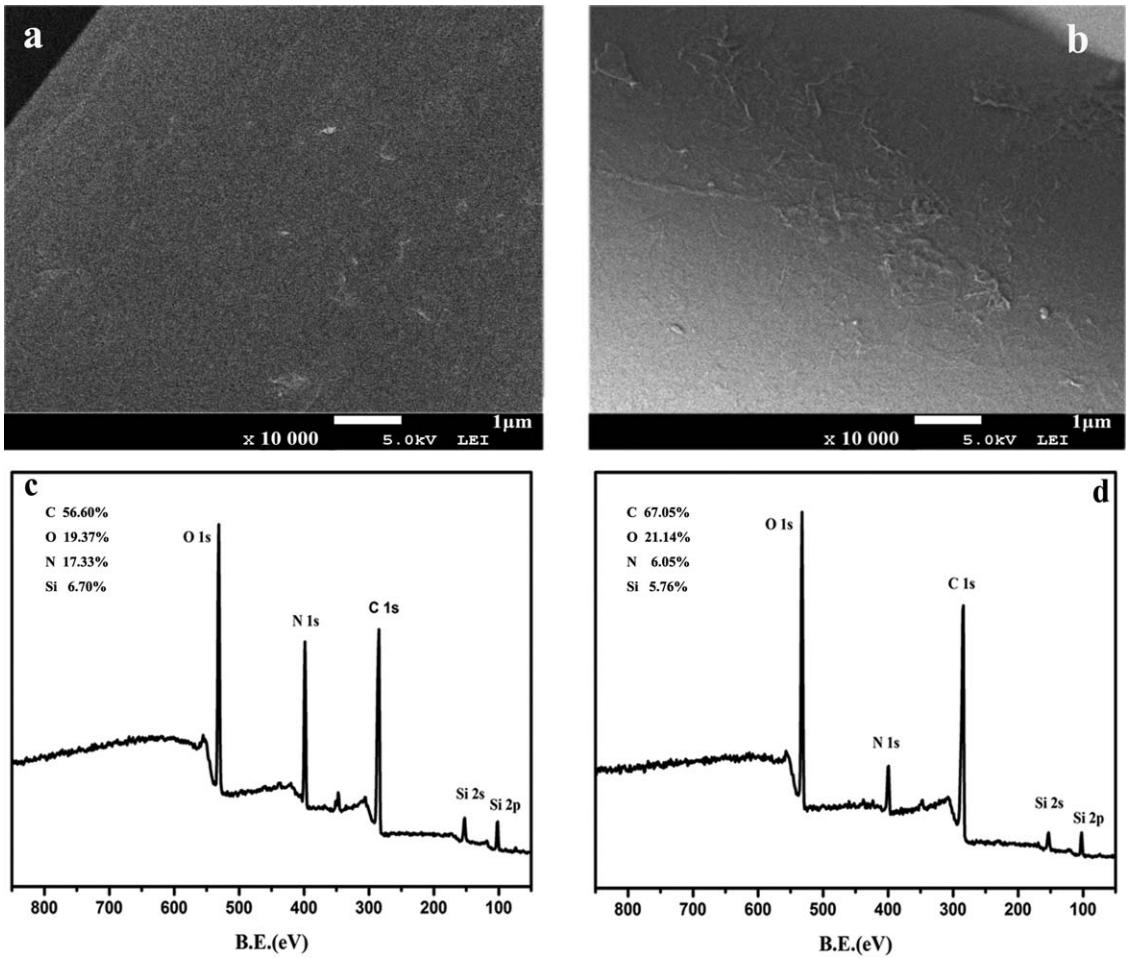

Figure 3. SEM morphology of original GF/APTES (a) and GF/CRG (b); XPS spectra of GF/APTES (c) and GF/CRG (d).

Preparation of GF/CRG

Prior to preparation of GF/CRG, the glass fiber was treated at 120°C to eliminate the organic remnant.[27] 1 g GF was firstly dispersed in 200 ml ethanol and 1 wt % ATPES[28] was added slowly accompanied with agitation at 35°C. After 1 h, GF was filtered from the mixture and cured in vacuum at 80°C for 6 h. And then this positively charged glass fiber was dispersed into 200 ml GO aqueous solution (0.05 mg/ml) and mildly stirred for 2 h. The color of GO solution faded gradually and GF was coated with a layer of GO accordingly.[29,30] The GF/CRG material was finally obtained through chemical reduction with 200 ml ascorbic acid (1 mg/ml) at 40°C under stirring for 12 h.[31]

Table I. Element Content of Different Fiber Surface Calculated from XPS Spectra

	Element content (%)			
Sample	C	O	N	Si
GF/APTES	56.60	19.37	17.33	6.70
GF/CRG	67.05	21.14	6.05	5.76
GF/CRG after processing	63.94	27.17	3.76	5.14

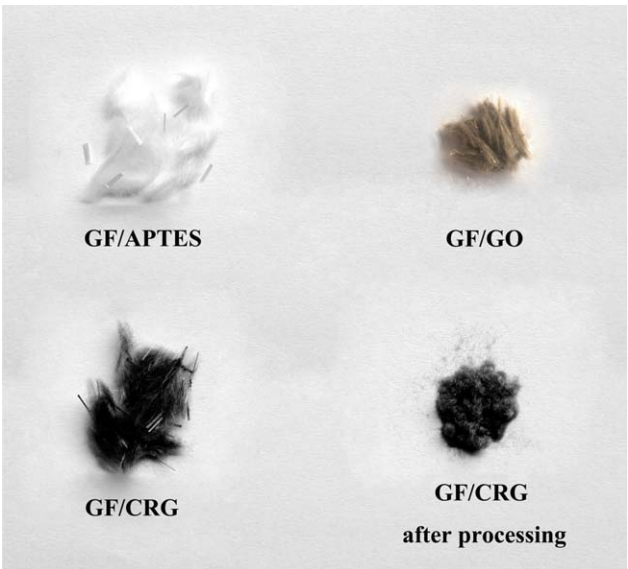

Figure 4. A photograph of different GF: GF/APTES, GF/GO, GF/CRG, and GF/CRG after processing. [Color figure can be viewed in the online issue, which is available at wileyonlinelibrary.com.]

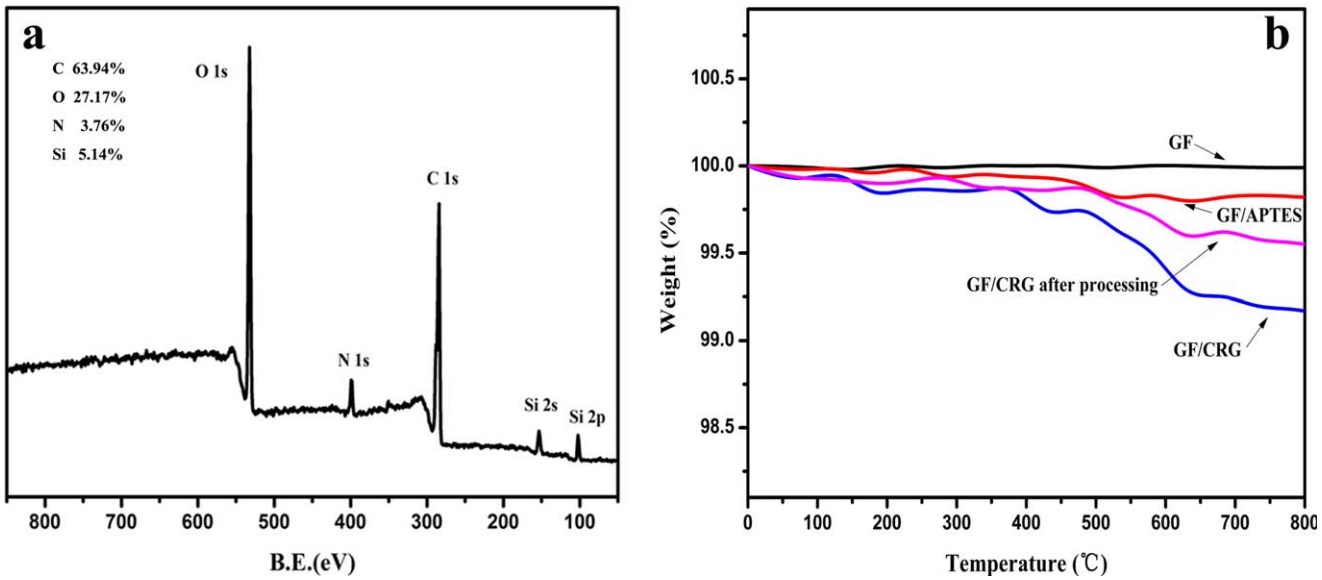

Figure 5. XPS spectra of GF/CRG after processing and TGA curves of samples. [Color figure can be viewed in the online issue, which is available at wileyonlinelibrary.com.]

Preparation of PLA Composites

The composites of PLA and modified glass fiber (PLA–GF/CRG) were prepared by melt blending with a plastic mixer machine (HAAKE PolyLab OS RhenDrive16 and HAAKE Rheomix OS, Germany) at 180°C. The composites of PLA with 5 wt % GF/CRG, 10 wt % GF/CRG were prepared in this paper, and PLA/untreated glass fiber composites (PLA–GF) with the same content were also prepared to make a comparison.

Characterization

Images of GO were examined by a Nanoscope Multimode and Explore atomic force microscope (AFM, Vecco Instruments) with TESP silicon tips. GO was dispersed in water for an extremely diluted concentration and the solution was dropped to a fresh mica sheet, and then dried sufficiently to prepare the samples for AFM.

The morphology of the polymer material was observed by field-emission scanning electron microscopy (SEM, JSM-7500F, JEOL, Japan) at a 5 kV accelerating voltage. The composites were cryogenically fractured in liquid nitrogen. And then the surfaces were coated with gold before observation.

X-ray photoelectron spectroscopy (XPS) measurements were performed with an XSAM800 (Kratos Company, UK) using Al Kα radiation; CasaXPS software was used to calculate the atomic concentrations and XPSpeak41 was used to perform curve fitting. A normal Lorentzian–Gaussian (80) was adopted.

Thermogravimetric analysis (TGA) was conducted by TA Q600 (TA Company). Each sample of approximately 5 mg was

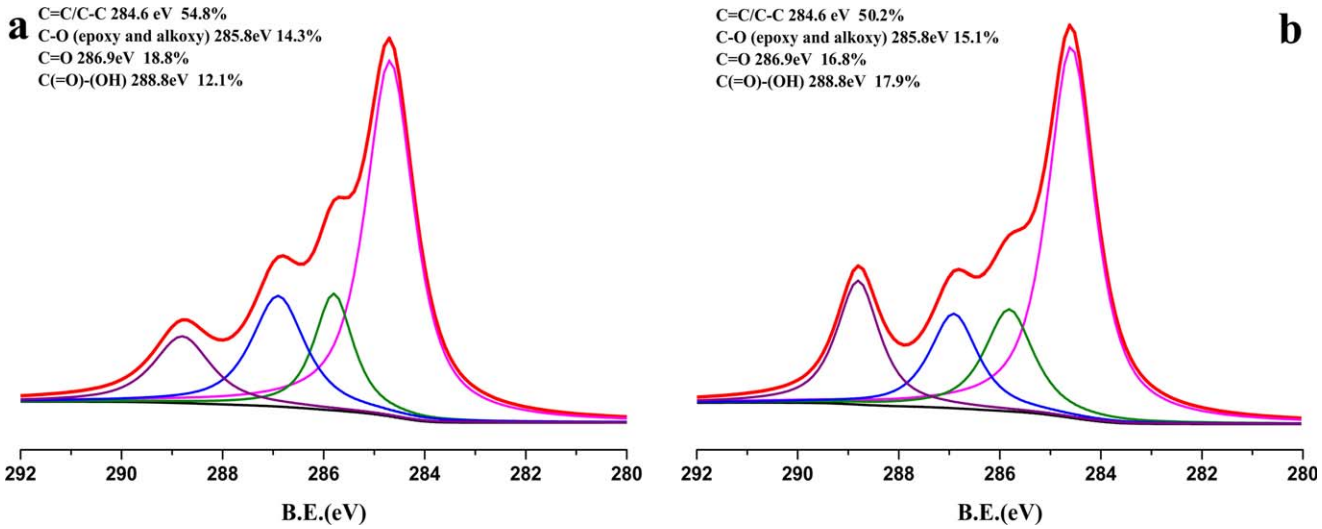

Figure 6. C1s XPS spectra of GF/CRG (a) and GF/CRG after processing (b). [Color figure can be viewed in the online issue, which is available at wileyonlinelibrary.com.]

measured in an aluminum crucible under air atmosphere from room temperature to 800°C at the heating rate of 10°C/min. The value of each sample was obtained as the average of at least three times.

The crystal structure of composites was determined with an X-ray diffractometer (Philip X pert PRO MPD, Panalytical, The Netherlands) with a Cu target and a rotating anode generator operated at 40 kV and 40 mA. The scanning rate was $2°min^{-1}$ from 5° to 40°.

The crystallization of neat PLA and its composites were recorded by differential scanning calorimetry (DSC, NETZSCH DSC-204F1, Germany). The samples weighted from 6 to 8 mg were first heated from room temperature to 200°C at a rate of 20°C min^{-1}, and then held at this temperature for 5 min to eliminate any residual thermal history, subsequently, cooled to 30°C at a rate of 10 and 2°C min^{-1}, respectively, to obtain the different rate cooling curves. At last, the samples were heated rapidly from 30 to 200°C (10°C min^{-1}). All experiments were performed under nitrogen.

The tensile strength of the prepared samples was determined using universal testing machine (Instron 5567) at constant crosshead speed of 30 mm/min at room temperature. The samples were cut into 75 mm × 40 mm × 4 mm according to ASTM D638 standard. Load of 1.0 kN was applied in the experiments. Five tests were taken for the average value to collect the results.

RESULTS AND DISCUSSION

Electrostatic Self-Assembly of Graphene

GO was synthesized successfully by the modification of Hummers and Offeman's method. As confirmed by AFM, the thickness of GO is 1–1.5 nm and it can be regarded as single laye.[32,33] The size is about 0.5 μm as shown in the height profile diagram of Figure 1. The remarkable diffraction signals of XRD is at 10.6°, corresponding to the d001 spacing with a distance of 8.6 Å, which is larger than the normal interlayer spacing of graphite, due to the presence of oxide groups in GO surface. No peak at around 26° is detected, indicating that graphite is oxidized totally to GO.[34] And the content of oxygen element is 29.26% as shown in Figure 1(c) of the XPS results.

The GF/CRG was constructed in terms of the mechanism showed in Figure 2. The surfaces of GF/APTES and GF/CRG were observed by SEM. The roughened textures of GF surface in GF/CRG indicate that CRG is successfully coated on GF surface. GO can be linked to the amino surfaces of glass fiber in the following way: protonation of the amine by the weakly acidic sites of the GO layers (COO^- ^+H_3N—R) and electrostatic attraction between the oppositely charged ions.[35] The graphene on the surface of GF obtained by the chemical reduction can act as nucleating agent to induce interfacial crystallization of polymer and improve the interfacial adhesion.[21,36]

XPS[37,38] was utilized to analyze the change of superficial element content of GF before and after electrostatic assembly of graphene. As shown in Figure 3 and Table I, the increased carbon content calculated from XPS spectra of the samples indicates that surface of GF/CRG fiber is successfully coated with

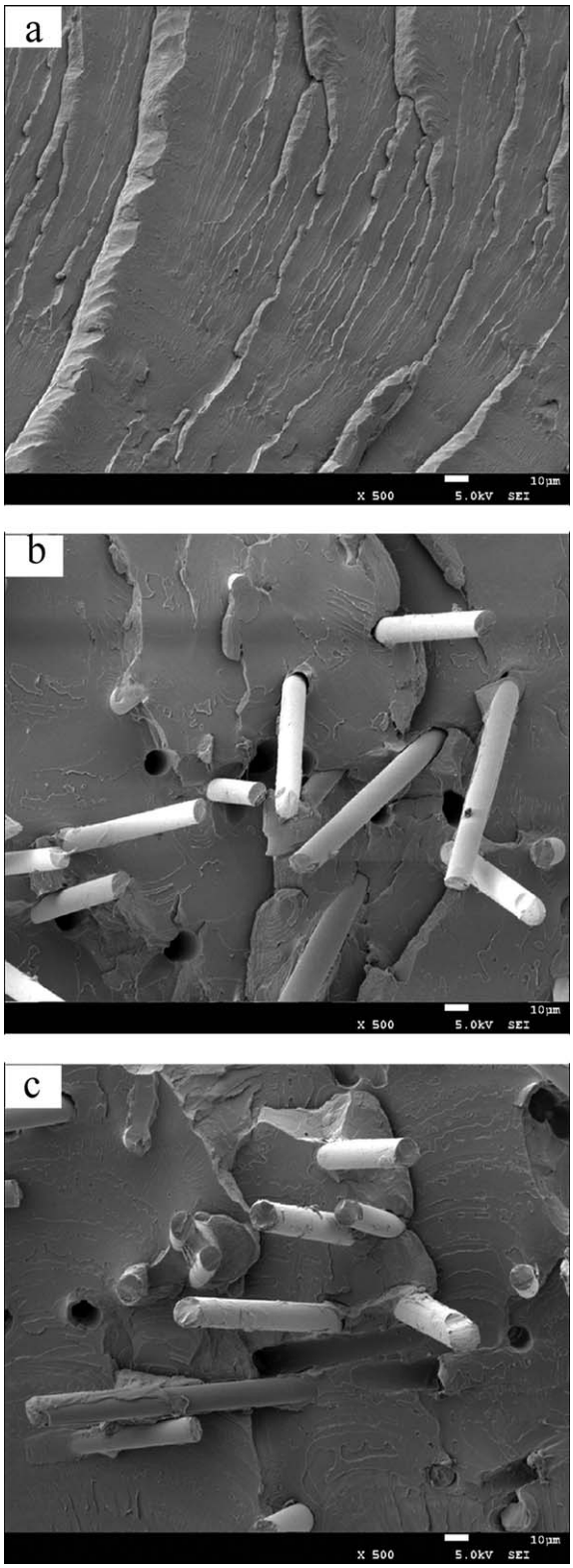

Figure 7. SEM images of the fractured surface of PLA–NEAT (a), PLA–GF (b), and PLA–GF/CRG (c). The scale bars are 10 μm.

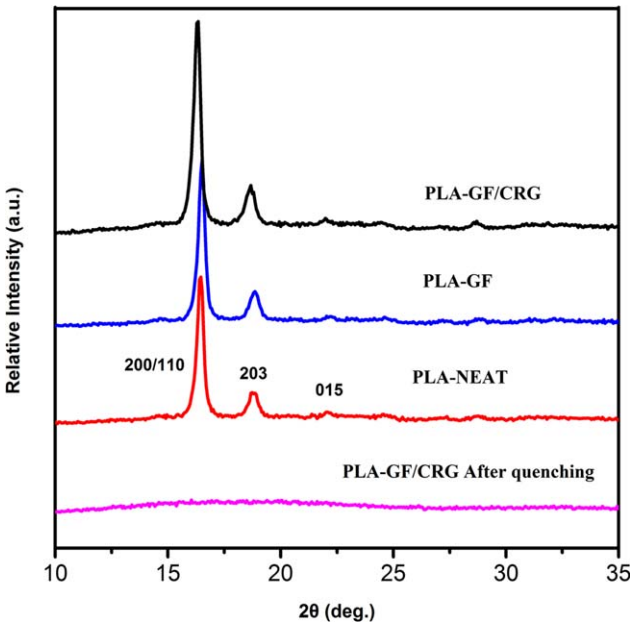

Figure 8. XRD patterns of the PLA sample and the composites before and after crystallization at 110°C. [Color figure can be viewed in the online issue, which is available at wileyonlinelibrary.com.]

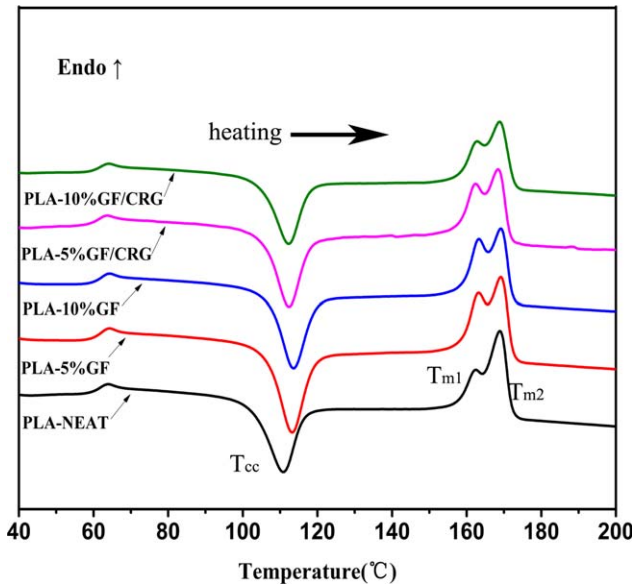

Figure 9. DSC analyses of samples in the second heating process (10°C/min) after a cooling process (10°C/min). [Color figure can be viewed in the online issue, which is available at wileyonlinelibrary.com.]

graphene through electrostatic interaction. The terminal amino group is covered by a layer of graphene, causing the sharp reduce of nitrogen content in XPS signal.

The PLA composites with this kind of functionalized GF were prepared via melt blending. Figure 4 demonstrated the direct changes of GF in self-assembly and processing procedure. After self-assembly, GF was coated with graphene and the color of GF was darken. GF/CRG of the processed PLA composites was extracted by chloroform for 24 h.[39] As shown in the figure of extracted GF/CRG (after melt blending), the black color of the shorter GF/CRG fiber suggests that a lot of graphene was kept on the surface of the fiber.

The TGA curves of GF, GF/APTES, GF/CRG and GF/CRG after processing under air atmosphere are shown in Figure 5. Almost no mass loss in neat fiber from room temperature to 800°C suggests that there were few functional groups and carbon element in the original fiber. Most carbon and oxygen groups begin to burn from 400°C[40] and we can estimate the coating contents via the weight loss. As we can see, the content of graphene in the surface of GF/CRG is about 0.7% and that in GF/CRG after processing is about 0.4%. Part of the graphene (almost 43%) fell off during the melt-blend and afterwards extraction.

The XPS spectrum demonstrates that GF/CRG after processing is comprised 63.94% C and 27.16% O. The C1s spectra in Figure 6 were compared by deconvoluting each spectrum into four peaks that correspond to the following functional carbon groups: C═C/C—C (284.6 eV), C—O (285.8 eV), C═O (286.9 eV), and C(═O)—(OH) (288.8 eV).[41] Clearly, more carboxylates groups were found after processing, which suggests that graphene was further exfoliated and exposed oxygen-rich inner surface. Although some graphene was erased during processing and extraction, more than half (57%) was still left on the surface of GF.

Application in PLA Composite

The dispersion of glass fiber in PLA matrix was observed by SEM. As shown in Figure 7, SEM micrographs revealed a good dispersion of glass fiber in composites. Some glass fibers were pulled out with holes left and some were fractured. Obviously, CRG had stronger adhesive force with PLA matrix and visible PLA material adhered to the surface of glass fiber. The special structure of nanoparticle surface which lacks adjacent coordination atoms is prone to agglomeration especially in melt process. Through attachment of graphene to glass fiber, graphene is well-distributed in matrix and induces interfacial crystallization of polymer on the surface of fiber which improves the interfacial interaction.

Figure 8 shows X-ray diffraction (XRD) patterns of neat PLA and its composites before and after crystallization. No characteristic peak was observed for the PLA–GF/REG after quenching, which confirms the entirely amorphous morphology of the sample. After crystallization at 110°C, the samples exhibit remarkable diffraction signals: The strongest peak at 16.6° was

Table II. Calorimetric Data Derived from the Second Heating (10°C/min) DSC Scan from the PLA–NEAT and its Composites

Sample	T_g (°C)	T_{cc} (°C)	$\triangle H$ (J/g)	T_{m1} (°C)	T_{m2} (°C)	X_c (%)
PLA-NEAT	61.6	110.9	6.08	162.4	168.9	6.49
PLA-5%GF	61.9	113.2	5.85	163.2	169.1	6.57
PLA-5%GF/CRG	61.9	112.4	5.98	162.4	168.4	6.72
PLA-10%GF	61.9	113.6	6.32	163.3	169.2	7.49
PLA-10%GF/CRG	61.9	112.3	6.40	162.8	168.8	7.59

Table III. Calorimetric Data Derived from the Cooling Process (2°C/min) and Second Heating (10°C/min) DSC Scan from the PLA–NEAT and its Composites

Sample	T_g (°C)	T_c (°C)	$\triangle H_c$ (J/g)	$\triangle H_m$ (J/g)	X_c (%)
PLA-NEAT	57.8	102.9	25.87	36.44	27.61
PLA-5%GF	58.0	103.2	28.78	36.84	32.33
PLA-5%GF/CRG	58.0	106.0	34.83	45.54	39.13
PLA-10%GF	58.0	107.1	37.79	48.34	44.81
PLA-10%GF/CRG	57.8	110.5	43.25	55.37	51.29

due to reflections from (200) and/or (110) planes, and the less intense peaks at 18.9° and 22.1° were attributed to reflections of the (203) and (015) planes of the α crystal of PLA, respectively.[42–44] According to the similar XRD patterns, the crystalline structure and lattice parameter among the samples were almost not changed. The attachment of graphene to the glass fiber surfaces made stronger and wider crystalline peaks, illustrating a higher degree of crystallinity of PLA–GF/CRG composites.

The glass transition and crystallization/melting phenomena of PLA and its composites were investigated by DSC analysis. Figure 9 shows the second heating DSC curves of the samples after quenching. The glass transition temperature (T_g), cold crystallization temperature (T_{cc}), melt temperature (T_{m1}, T_{m2}) are listed in Tables II and III. The crystallinity (X_c) of PLA and composites is evaluated using equation $Xc\ (\%) = \triangle H/((1-\phi)\triangle H^*) \times 100\%$ where $\triangle H = \triangle H_m - \triangle H_{cc}$ (for second heating curves, as $\triangle H_m$ is the specific melting enthalpy of the sample, $\triangle H_{cc}$ is the specific cold crystallization enthalpy of the sample). $\triangle H^*$ is the melting enthalpy of the 100% crystalline polymer matrix (93.7 J/g for PLA[45,46]) and ϕ is the total weight percentage of GF or GF-CRG.

It could be seen that the cold-crystallization temperature (T_{cc}) of PLA increases in the presence of glass fiber and the T_{cc} of PLA–GF is higher than that of PLA–GF/CRG sample with the same filler content. This illustrates that the presence of glass fiber and graphene reduces PLA chain mobility and hinders crystal growth.[47] At the same time, due to the outstanding nucleating effect of graphene the cold-crystallization peak temperature of PLA shifts downward for PLA–GF/CRG compared to that for PLA–GF composites. No exothermic events other than the glass transition during the cooling scan were observed and the crystallinity (X_c) calculated by second heating curves increased a little, which suggests that the PLA was difficult to crystallize from the molten state in the fast nonisothermal quenching process even in the presence of graphene. These data illustrate that the presence of glass fiber and graphene reduces PLA chain mobility and hinders crystal growth dominantly in cold crystallization.

The DSC thermograms recorded during slow cooling and second heating of PLA composites are reported in Figure 10, respectively. The data derived from DSC analyses are reported in Table III. T_c is the crystallization temperature and $\triangle H_c$ is crystallization enthalpy in the cooling process. $\triangle H_m$ is the specific melting enthalpy of the sample evaluated by second heating curves. $X_c\ (\%) = \triangle H_c/((1-\phi)\triangle H^*) \times 100\%$ (for cooling curves, as $\triangle H_c$ is the specific crystallization enthalpy of the sample).

From Figure 10 and Table III, could we could know that there was obviously melt crystallization in the cooling process at a slow cooling rate (2°C/min). These phenomena may be caused by the slow cooling rate and nucleating effect. The crystallinity of PLA–GF/CRG was much higher than neat PLA, and even than PLA–GF composites, showing a higher crystallization temperature at the same time. The graphene nanosheets could act as a heterogeneous nucleating agent[48] during melt crystallization

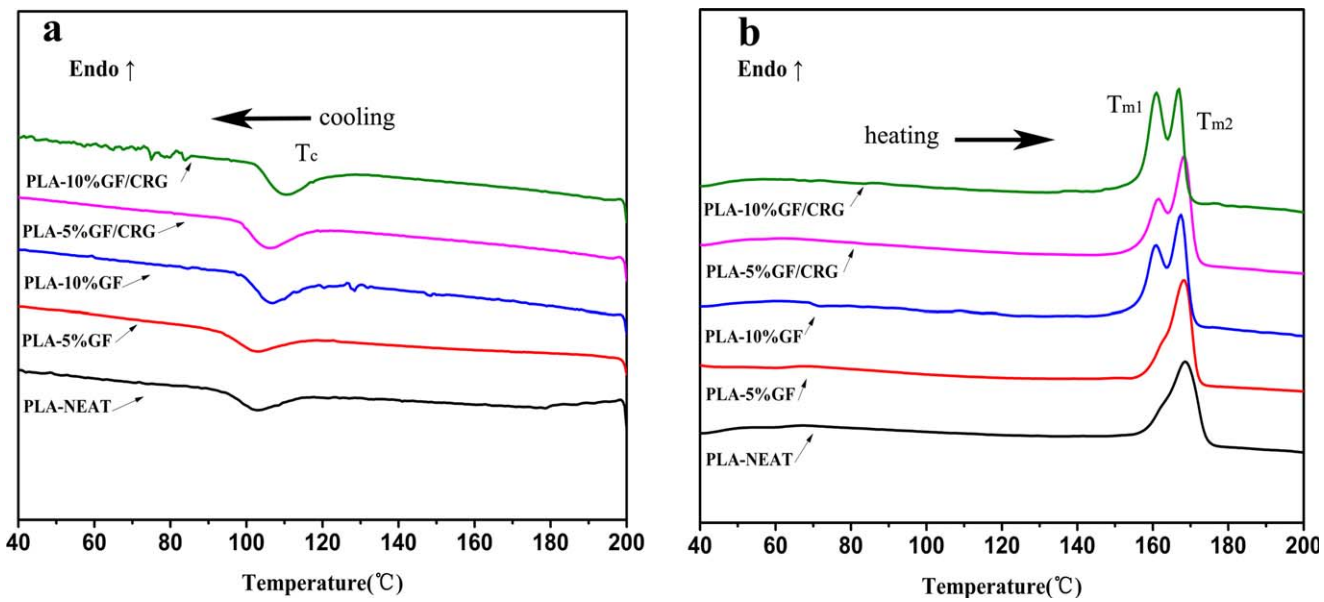

Figure 10. DSC analyses of samples in the cooling process (2°C/min) (a) and second heating process (10°C/min) (b). [Color figure can be viewed in the online issue, which is available at wileyonlinelibrary.com.]

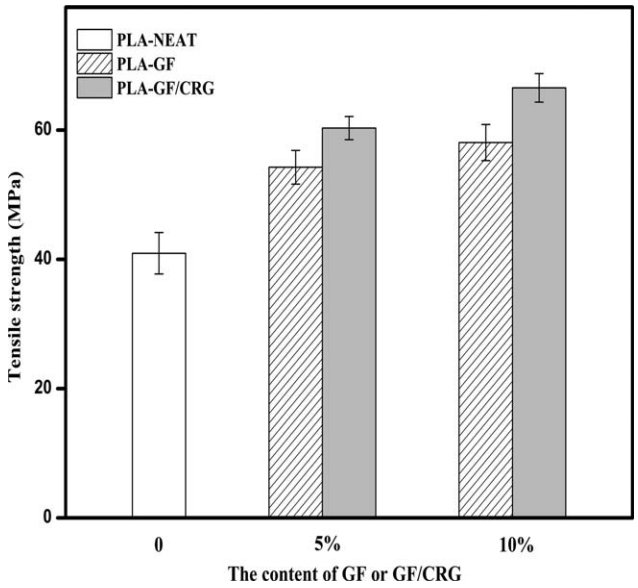

Figure 11. Tensile uniaxial tensile testing of PLA and PLA composites.

and induce the generation and growth of PLA spherulite. And this nucleating effect accelerated the crystallization process of PLA at a higher temperature. This illustrated that the method we used in this experiment to prepared PLA–GF/REG composites was effective to increase the crystallinity rate and the crystallization temperature.

To evaluate the composite's mechanical performance, uniaxial tensile testing on tension samples was conducted. The results of uniaxial tensile testing of the baseline PLA and composite samples are shown in Figure 11. The weight fraction of GF and graphene in the PLA matrix was held at 5 or 10% in total. The tensile strength of the PLA–GF/CRG composite (66.53 MPa) is about 63% larger than that of the pristine PLA (40.94 MPa). While PLA–GF (58.07 MPa) composite only shows 42% increase when the content of filler is 10%. A similar result is observed at a filler weight fraction of 5%. What is noteworthy to us, the graphene content in GF/CRG is 0.7%, an extremely low value. The reinforcement effect of GF/CRG on PLA is achieved by the strong adhesive force, good interfacial crystallization and excellent intrinsic property of GF/CRG. This illustrates the CRG modified GF can be used to prepare PLA composite with good mechanical performance.

CONCLUSIONS

In this work, graphene oxide is successfully prepared by the modification of Hummers and Offeman's method. It is used to prepare graphene coated GF (GF/CRG) material with glass fiber via electrostatic self-assembly. PLA–GF/CRG composites are prepared by melt-blending. The comparison between GF/CRG before and after blending process indicates that most graphene is firmly adsorbed by the positively charged GF. The graphene on the surface of GF could have a prominent influence on the property of PLA matrix. On the one hand, the presence of graphene has a significant influence on both the cold and melt crystallizations of PLA (increases crystallization temperature and crystallinity obviously, accelerates the crystallization process) which reveals the outstanding heterogeneous nucleating effect of graphene. On the other hand, even an extremely small amount of graphene could greatly improve the mechanical properties of PLA matrix. Good mechanical property of PLA–GF/CRG is achieved by the strong adhesive force, good interfacial crystallization and excellent intrinsic property of GF/CRG. The electrostatic self-assembly method in this experiment is effective to make high performance composites.

REFERENCES

1. Novoselov, K. S.; Geim, A. K.; Morozov, S. V.; Jiang, D.; Zhang, Y.; Dubonos, S. V.; Grigorieva, I. V.; Firsov, A. A. *Science* **2004**, *306*, 666.
2. Geim, A. K.; Novoselov, K. S. *Nat. Mater.* **2007**, *6*, 183.
3. Kim, H.; Abdala, A. A.; Macosko, C. W. *Macromolecules* **2010**, *43*, 6515.
4. Steurer, P.; Wissert, R.; Thomann, R.; Muelhaupt, R. *Macromol. Rapid. Commun.* **2009**, *30*, 316.
5. Potts, J. R.; Dreyer, D. R.; Bielawski, C. W.; Ruoff, R. S. *Polymer* **2011**, *52*, 5.
6. Rafiee, M. A.; Rafiee, J.; Wang, Z.; Song, H.; Yu, Z. Z.; Koratkar, N. *ACS Nano* **2009**, *3*, 3884.
7. Morozov, S. V.; Novoselov, K. S.; Katsnelson, M. I.; Schedin, F.; Elias, D. C.; Jaszczak, J. A.; Geim, A. K. *Phys. Rev. Lett.* **2008**, *100*, 016602.
8. Lee, C.; Wei, X. D.; Kysar, J. W.; Hone, J. *Science* **2008**, *321*, 385.
9. Balandin, A. A.; Ghosh, S.; Bao, W. Z.; Calizo, I.; Teweldebrhan, D.; Miao, F.; Lau, C. N. *Nano Lett.* **2008**, *8*, 902.
10. Lee, S. H.; Kim, H. W.; Hwang, J. O.; Lee, W. J.; Kwon, J.; Bielawski, C. W.; Ruoff, R. S.; Kim, S. O. *Angew. Chem. Int. Ed.* **2010**, *49*, 10084.
11. Chen, W. F.; Li, S.; Chen, C. H.; Yan, L. F. *Adv. Mater.* **2011**, *23*, 5679.
12. Yan, J.; Wang, Q.; Wei, T.; Jiang, L.; Zhang, M.; Jing, X.; Fan, Z. *ACS Nano* **2014**, *8*, 4720.
13. Ismach, A.; Druzgalski, C.; Penwell, S.; Schwartzberg, A.; Zheng, M.; Javey, A.; Bokor., J.; Zhang, Y. *Nano Lett.* **2011**, *10*, 1542.
14. Xu, Z.; Gao, C. *Nat. Commun.* **2011**, *2*, 571.
15. Kim, G. Y.; Choi., M. C.; Lee, D.; Ha, C. S. *Macromol. Mater. Eng.* **2012**, *297*, 303.
16. Li, C.; Shi, G. *Nanoscale* **2012**, *4*, 5549.
17. Xu, Y.; Wu, Q.; Sun, Y.; Bai, H.; Shi, G. *ACS Nano* **2010**, *4*, 7358.
18. Zhu, Y.; Murali, S.; Cai, W.; Li, X.; Suk, J. W.; Potts, J. R.; Ruoff, R. S. *Adv. Mater.* **2010**, *22*, 3906.
19. Li, Z.; Wang, J.; Liu, X.; Liu, S.; Ou, J.; Yang, S. *J. Mater. Chem.* **2011**, *21*, 3397.
20. Shen, J.; Hu, Y.; Li, C.; Qin, C.; Shi, M.; Ye, M. *Langmuir* **2009**, *25*, 6122.

21. Ning, N.; Zhang, W.; Yan, J.; Xu, F.; Wang, T.; Su, H.; Tang, C.; Fu, Q. *Polymer* **2013**, *54*, 303.
22. Nampoothiri, K. M.; Nair, N. R.; John, R. P. *Bioresour. Technol.* **2010**, *101*, 8493.
23. Barletta, M.; Vesco, S.; Puopolo, M.; Tagliaferri, V. *Prog. Org. Coat.* **2015**, *8*, 13.
24. Barletta, M.; Puopolo, M.; Tagliaferri, V.; Vesco, S. *J. Appl. Polym. Sci.* **2015**, *132*, 42252.
25. Barletta, M.; Vesco, S.; Puopolo, M.; Tagliaferri, V. *Surf. Coat. Technol.* **2015**, *272*, 322.
26. Hummers, W. S., Jr.; Offeman, R. E. *J. Am. Chem. Soc.* **1958**, *80*, 1339.
27. Li, Z. F.; Ruckenstein, E. *J. Colloid. Interface Sci.* **2002**, *251*, 343.
28. Li, C.; Liu, X. *Mater. Lett.* **2007**, *61*, 2239.
29. Becerril, H. A.; Mao, J.; Liu, Z.; Stoltenberg, R. M.; Bao, Z.; Chen, Y. *ACS Nano* **2008**, *2*, 463.
30. Li, W.; Chen, B.; Meng, C.; Fang, W.; Xiao, Y.; Li, X.; Hu, Z.; Xu, Y.; Tong, L.; Wang, H.; Liu, W.; Bao, J.; Shen, Y. R. *Nano Lett.* **2014**, *14*, 955.
31. Zhang, J.; Yang, H.; Shen, G.; Cheng, P.; Zhang, J.; Guo, S. *Chem. Commun.* **2010**, *46*, 1112.
32. Stankovich, S.; Dikin, D. A.; Piner, R. D.; Kohlhaas, K. A.; Kleinhammes, A.; Jia, Y.; Wu, Y.; Nguyen, S. T.; Ruoff, R. S. *Carbon* **2007**, *45*, 1558.
33. Xu, Y.; Bai, H.; Lu, G.; Li, C.; Shi, G. *J. Am. Chen. Soc.* **2008**, *130*, 5856.
34. Marcano, D. C.; Kosynkin, D. V.; Berlin, J. M.; Sinitskii, A.; Sun, Z.; Slesarev, A.; Alemany, L. B.; Lu, W.; Tour, J. M. *ACS Nano* **2010**, 484806.
35. Kovtyukhova, N. I.; Ollivier, P. J.; Martin, B. R.; Mallouk, T. E.; Chizhik, S. A.; Buzaneva, E. V.; Gorchinskiy, A. D. *Chem. Mater.* **1999**, *11*, 771.
36. Han, S.; Ren, K.; Geng, C.; Wang, K.; Zhang, Q.; Chen, F.; Fu, Q. *Polym. Int.* **2014**, *63*, 646.
37. Yang, D.; Velamakanni, A.; Bozoklu, G.; Park, S.; Stoller, M.; Piner, R. D.; Stankovich, S.; Jung, I.; Field, D. A.; Ventrice, C. A., Jr.; Ruoff, R. S. *Carbon* **2009**, *47*, 145.
38. Panchakarla, L. S.; Subrahmanyam, K. S.; Saha, S. K.; Govindaraj, A.; Krishnamurthy, H. R.; Waghmare, U. V.; Rao, C. N. R. *Adv. Mater.* **2009**, *21*, 4726.
39. Murariu, M.; Ferreira, A. D. S.; Degée, P.; Alexandre, M.; Dubois, P. *Polymer* **2007**, *48*, 2613.
40. Wang, G.; Yang, J.; Park, J.; Gou, X.; Wang, B.; Liu, H.; Yao, J. *J. Phys. Chem. C* **2008**, *112*, 8192.
41. Stankovich, S.; Piner, R. D.; Chen, X.; Wu, N.; Nguyen, S. T.; Ruoff, R. S. *J. Mater. Chem.* **2006**, *16*, 155.
42. Sabzi, M.; Jiang, L.; Liu, F.; Ghasemi, I.; Atai, M. *J. Mater. Chem. A* **2013**, *1*, 8253.
43. Mano, J. F.; Wang, Y.; Viana, J. C.; Denchev, Z.; Oliveira, M. J. *Macromol. Mater. Eng.* **2004**, *289*, 910.
44. Nam, J. Y.; Okamoto, M.; Okamoto, H.; Nakano, M.; Usuki, A.; Matsuda, M. *Polymer* **2006**, *47*, 1340.
45. Fukada, E. *Biorheology* **1995**, *32*, 593.
46. Turner, J. F.; Riga, A.; O' Connor, A.; Zhang, J.; Collis, J. *J. Therm. Anal. Calorim.* **2004**, *75*, 257.
47. Li, Y.; Sun, X. S. *Biomacromolecules* **2010**, *11*, 1847.
48. Wu, D.; Cheng, Y.; Feng, S.; Yao, Z.; Zhang, M. *Indus. Eng. Chem. Res.* **2013**, *52*, 6731.